Research Square

Preprints are preliminary reports that have not undergone peer review.
They should not be considered conclusive, used to inform clinical practice,
or referenced by the media as validated information.

A Wideband Antenna-Combined Doherty Power Amplifier With Integrated Output Power Combining

Mahesh A

maheshа@rvce.edu.in

R.V. College of Engineering

Kiran Kumar N S

R.V. College of Engineering

Prasidh Ramabadran

Sequans Communications (United Kingdom)

Article

Keywords:

Posted Date: November 23rd, 2026

DOI: https://doi.org/10.21203/rs.3.rs-11629684/v1

License: This work is licensed under a Creative Commons Attribution 4.0 International License.
Read Full License

Additional Declarations: No competing interests reported.

A Wideband Antenna-Combined Doherty Power Amplifier With Integrated Output Power Combining

Mahesh A[1*], Kiran Kumar N S[1†] and Prasidh Ramabadran[2†]

[1*]ECE, RV College of Engineering, Mysuru Road, Bengaluru, 560059, Karnataka, India.

[2]Principal RF/PHY System Architect, Sequans Communications Ltd., , City, 610101, State, United Kingdom.

*Corresponding author(s). E-mail(s): mahesha@rvce.edu.in;
Contributing authors: kirankumarns.rshast@rvce.edu.in;
pramabadran@sequans.com;
†These authors contributed equally to this work.

Abstract

This work presents an antenna-combined Doherty power amplifier (DPA) operating at 3.7 GHz, in which a dual-feed stacked-patch antenna is employed as both the output-combining and radiating element. Unlike a conventional DPA, where the carrier and peaking amplifier outputs are combined using a dedicated output-combining network before being connected to the transmitting antenna, the proposed architecture directly connects the two amplifier branches to separate feeds of the same antenna. This approach enables power combining and radiation within a common structure while reducing the need for a separate output-combining network. The proposed architecture is systematically compared with a conventional DPA, a conventional DPA with the transmitting antenna, and a transformer-based DPA to verify the Doherty load-modulation operation and assess the effect of replacing the conventional output-combining network. The proposed antenna-combined DPA achieves an impedance bandwidth of 1.11 GHz, compared with 260 MHz for the conventional DPA and 320 MHz for the conventional DPA with antenna. A peak large-signal gain of 12.4 dB, peak drain efficiency of 80%, and peak power-added efficiency of 67% are obtained, with a saturated output power of 42.2 dBm. The proposed antenna-combined DPA architecture preserves the characteristics of Doherty operation while providing

substantial bandwidth enhancement and improved efficiency, thereby demonstrating the feasibility of a compact and broadband antenna-combined DPA. The proposed architecture can be used for integration in active antenna arrays for high EIRP (Effective Isotropic Radiated Power) applications.

Keywords: Doherty power amplifier, antenna-integrated power amplifier, antenna-based power combining, dual-feed stacked patch antenna, broadband power amplifier, load modulation, drain efficiency, power-added efficiency.

1 Introduction

The rapid development of modern wireless communication systems has increased the demand for radio-frequency (RF) transmitters capable of providing high output power, high efficiency, and wide operating bandwidth. The use of spectrally efficient modulation schemes generally results in signals with high peak-to-average power ratio (PAPR), forcing the power amplifier (PA) to operate over a wide range of output power levels. Conventional PAs provide their highest efficiency close to saturation and exhibit reduced efficiency when operated at power back-off (PBO). Therefore, improving the efficiency of RF PAs over a wide output-power range while maintaining broadband operation has become an important research objective for modern wireless transmitters. The Doherty power amplifier (DPA), consisting primarily of carrier and peaking amplifier branches, provides an effective solution to this problem through active load modulation, enabling enhanced efficiency at output-power back-off. Consequently, considerable research has been devoted to improving the bandwidth, efficiency, linearity, and back-off range of DPA architectures for broadband wireless applications [1–6].

The bandwidth of a conventional DPA is strongly influenced by its output load-modulation network, impedance transformation, and the relative phase relationship between the carrier and peaking amplifier branches. The conventional quarter-wavelength impedance inverter and associated matching networks exhibit frequency-dependent characteristics, which restrict the achievable bandwidth and increase the physical size of the amplifier. To overcome these limitations, several broadband DPA techniques have been proposed. Modified load-modulation networks have been investigated to simultaneously extend the operating bandwidth and efficiency back-off range [1], while coupled phase-compensation networks have been introduced to compensate for frequency-dependent phase variations and improve broadband load modulation [2]. Simplified output-matching topologies have also been proposed to reduce circuit complexity and physical size while maintaining broadband impedance transformation [3]. Other approaches have employed supply-voltage and input-excitation adaptation to obtain reduced sensitivity to load variation [4], three-way load modulation for enhanced back-off performance [5], and reconfigurable quasi-balanced structures for multiband and mismatch-resilient operation [6]. These developments demonstrate that the output combining and matching network plays a critical role in determining the overall bandwidth and efficiency of a DPA.

Recent investigations have further explored compact load networks, asymmetric architectures, multimode operation, phase compensation, harmonic control, and alternative impedance transformation techniques to overcome the limitations of conventional DPA structures [7–14]. A 5-W GaN DPA with a wide operating bandwidth has demonstrated the applicability of broadband load modulation to high-frequency satellite communication systems [7]. Virtual-stub and asymmetric structures have been investigated to extend the bandwidth of the load-modulation network while maintaining efficient operation [8]. Compact L-section-based load networks have also been developed to reduce the number of passive components and improve the physical integration of the amplifier [9]. At millimeter-wave frequencies, silicon and GaN DPA implementations have demonstrated the applicability of Doherty operation to higher-frequency wireless and satellite systems [10, 11]. Dual-passband, load-independent, and phase-compensated DPA architectures have subsequently been reported to address frequency-dependent impedance and phase variations [12–14]. These studies indicate that considerable progress has been achieved through optimization of the active amplifier and its electrical output network; however, the interface between the DPA output network and the transmitting antenna remains an important aspect of transmitter integration.

Further advances in DPA technology have focused on achieving broadband and highly integrated operation using advanced load-modulation techniques and semiconductor technologies. Ultra-broadband load-insensitive DPAs have been developed for 5G mobile-terminal applications [15], while extended-bandwidth architectures based on nonlinear current profiles and input-phase control have been reported to improve the back-off operating range [16, 17]. Harmonic-control techniques have also been investigated for improving the efficiency of broadband DPA implementations [18]. More recently, generalized asymmetric load-modulation architectures using hybrid voltage-current operation have demonstrated ultrawideband performance [19], and dual-wideband three-stage architectures have been investigated for simultaneous multi-band operation [20]. Broadband GaAs HBT DPAs employing lumped compensation and input-phase correction have further demonstrated the importance of phase control in achieving broadband operation [21]. High-linearity broadband architectures [22], reduced peaking-amplifier output impedance techniques [23], and reconfigurable output networks [24] have also been reported. Other recent studies have investigated ultrawideband output networks for mobile-terminal applications [25], fully integrated GaN three-stage DPAs for 6G broadband applications [26], harmonic-suppression post-matching networks [27], and broadband architectures without post-matching networks [28]. Although these techniques significantly improve the electrical performance of the DPA, conventional architectures generally retain a dedicated output-combining and matching interface between the amplifier and the antenna.

In a conventional transmitter, the output of the DPA is connected to the transmitting antenna through an output-combining or matching network, transmission lines, and other passive structures. The associated insertion loss contributes directly to the degradation of the overall transmitter efficiency. In addition, independently designing the DPA for a fixed load and subsequently designing the antenna for the same impedance does not fully exploit the interaction between the active amplifier and

the radiating structure. An alternative approach is therefore to integrate the antenna into the output-combining function of the DPA so that the antenna itself participates in the load-modulation process. This concept has been demonstrated using multi-port antenna structures. Iupikov *et al.* proposed a dual-fed planar inverted-F antenna (PIFA) with a nonsymmetric impedance matrix for Doherty transmitters, in which the antenna was designed to accommodate the different loading conditions associated with the carrier and peaking amplifier branches [29]. A cavity-backed patch antenna with distributed multi-port feeding was subsequently investigated to enable efficient integration of the antenna with a DPA and filtering structure [30]. These studies establish that a multi-port antenna can be considered as an integral part of the DPA output network rather than simply as a conventional 50 Ω terminating load.

Motivated by this research gap, the present work investigates a DPA architecture in which the antenna is connected directly to the amplifier output instead of being placed after a conventional combiner stage. The proposed antenna employs two separate feed ports, with one feed connected to the carrier amplifier branch and the other connected to the peaking amplifier branch, so that the antenna becomes part of the DPA output environment rather than a separate load connected through an additional passive feed network. This approach aims to reduce feed transmission losses and improve effective power transfer from the amplifier to the radiator, while also supporting bandwidth enhancement by removing post-combiner feed lines and extra matching sections that can introduce frequency-dependent limitations. At the same time, the direct dual-feed configuration requires careful co-design of the amplifier and antenna, since the input impedance at each feed, the mutual coupling between the two ports, and the phase relationship between the carrier and peaking branches directly influence the Doherty load modulation mechanism. Therefore, the proposed architecture is intended to preserve the efficiency advantage of the Doherty concept while enabling a compact, low-loss, and potentially broad-band RF front-end solution.

The novelty of this work lies in the direct integration of a dual-feed stacked patch antenna with the carrier and peaking branches of a DPA, allowing the antenna to simultaneously perform RF power combining and radiation and thereby eliminating the separate output-combining network and post-combiner interface. Unlike conventional antenna-loaded DPA configurations, the proposed architecture directly excites the two antenna feeds from the respective DPA branches, making the antenna an integral part of the Doherty load-modulation network. A transformer-based DPA is also investigated as an intermediate reference to validate the proposed output-combining concept. This approach enables significant impedance-bandwidth enhancement while maintaining comparable saturated output power and improved peak efficiency, demonstrating the potential of antenna-based power combining for compact and broadband RF transmitter architectures. Section II presents the design methodology of the proposed Doherty power amplifier and antenna system, including the amplifier design, antenna design, and their integration. The performance of the developed DPA and antenna-integrated configurations is evaluated in the section III through small-signal and large-signal analyses. The overall findings obtained from the performance evaluation are summarized in the section IV.

2 Design Methodology of the Proposed Doherty Power Amplifier and Antenna System

As illustrated in Fig. 1, the proposed DPA was developed through a systematic design procedure consisting of DC analysis,stability analysis, harmonic-balance analysis, load-pull and source-pull analysis, matching-network design, individual optimization of the carrier and peaking amplifiers, and final DPA implementation. The CGH40010F GaN HEMT transistor was selected for both the carrier and peaking amplifier branches because of its high gain, high efficiency, and wideband capability. Since the target operating frequency of this work is 3.7 GHz, the RF characteristics specified in the device datasheet at $f_0 = 3.7$ GHz were adopted for the design. Under the recommended operating conditions of $V_{DD} = 28$ V and $I_{DQ} = 200$ mA.

The transistor provides a typical small-signal gain of 14.5 dB, a saturated output power of 12.5 W, and a typical drain efficiency of 65%, making it well suited for DPA applications.

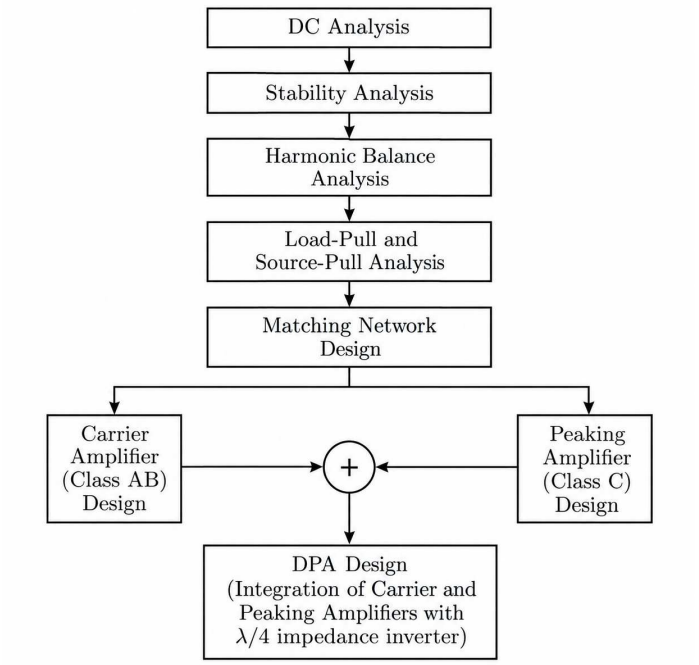

Fig. 1 Design procedure of the proposed Doherty power amplifier.

The design procedure begins with the DC analysis of both the carrier and peaking amplifier branches to establish the desired operating regions. The carrier amplifier was biased in Class AB with $V_{DS} = 28$ V and $V_{GS} = -2.7$ V to ensure continuous conduction and improved linearity over the low- and medium-power regions. The peaking amplifier was biased in Class C using the same drain voltage while reducing the gate voltage to $V_{GS} = -3.6$ V, thereby maintaining the device near cutoff. Since

the threshold voltage of the transistor is -3.0 V, this bias keeps the peaking amplifier inactive at low input power levels and allows it to conduct only as the input power approaches saturation, thereby enabling the Doherty load-modulation mechanism.

Following the bias design, stability analysis was performed because the CGH40010F is supplied as an unmatched transistor. To ensure unconditional stability over the operating frequency range, a 4 Ω resistor was incorporated into the stabilization network. This resistor effectively suppresses potential oscillations while preserving satisfactory gain characteristics, thereby providing a stable platform for subsequent large-signal optimization.

After confirming stable operation, harmonic-balance analysis was carried out under large-signal excitation to evaluate the nonlinear characteristics of both amplifier branches. The harmonic-balance simulation provides the output power, gain, drain efficiency, power-added efficiency, and waveform characteristics required to optimize the large-signal operation of the Class AB and Class C amplifiers.

Subsequently, load-pull and source-pull analyses were performed to determine the optimum source and load impedances corresponding to the selected bias conditions. These analyses are essential because the output power and efficiency of the transistor strongly depend on the impedance presented at its input and output terminals. For the carrier amplifier, the source and load impedances were obtained as $4.4 - j10.4$ Ω and $10.645 + j3.691$ Ω respectively. Similarly, for the peaking amplifier, the Source and load impedances were found to be $5.10 - j15.210$ Ω and $10.645 + j3.691$ Ω respectively. These impedance values served as the design targets for the matching networks.

Based on the optimum impedance values obtained from the load-pull and source-pull analyses, the input and output matching networks were designed to transform the standard 50 Ω system impedance to the optimum transistor impedances while maximizing gain, output power, and efficiency at the operating frequency. The optimized matching networks were then integrated with the respective transistor circuits to realize the final Class AB carrier amplifier and the final Class C peaking amplifier.

Finally, the optimized Class AB and Class C amplifier branches were integrated using a quarter-wavelength ($\lambda/4$) impedance inverter to realize the complete Doherty power amplifier architecture. The resulting DPA was subsequently employed for antenna integration and wireless performance evaluation, as presented in the following sections.

2.1 Conventional Doherty Power Amplifier

After the individual Class AB and Class C amplifiers were optimized, they were integrated to realize the DPA architecture. Fig. 2 shows the functional block diagram of the conventional DPA. The input signal P_{in} is first divided by a power splitter into two parallel signal paths, namely the carrier path and the peaking path. The carrier path consists of the Class AB amplifier, whereas the peaking path consists of a phase-compensation network followed by the Class C amplifier. This arrangement forms the basic Doherty structure, in which the two amplifiers operate together to improve efficiency over a wide output-power range.

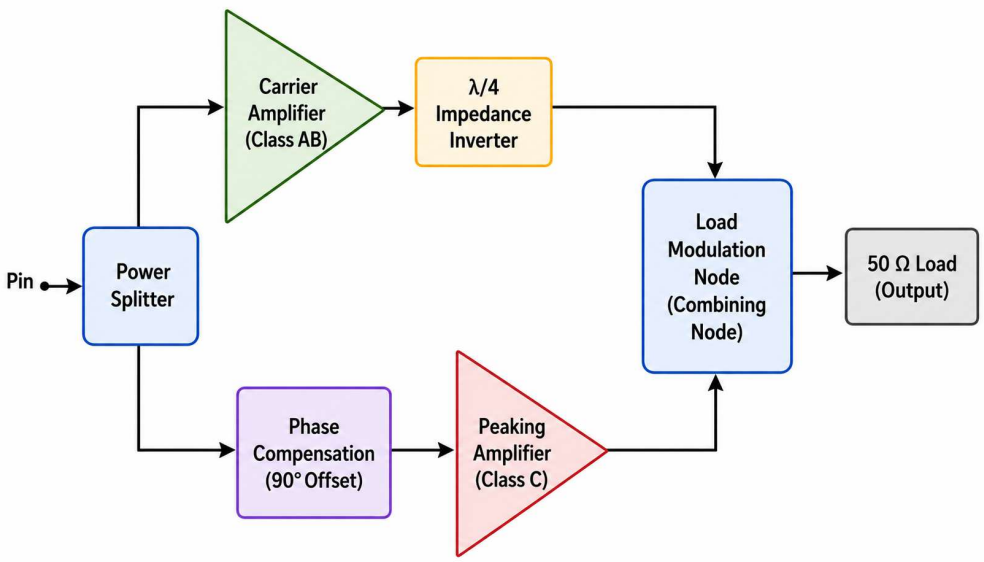

Fig. 2 Block diagram of the conventional DPA.

The upper branch contains the carrier amplifier, which is biased in Class AB and remains active throughout the entire operating range. Since the carrier amplifier conducts even at low input power levels, it is responsible for signal amplification in the low- and medium-power regions. After amplification, the output of the carrier branch is connected to a $\lambda/4$ impedance inverter. This quarter-wave transmission line is a key element of the Doherty architecture because it transforms the load impedance seen by the carrier amplifier and enables the required load-modulation mechanism.

The lower branch contains the peaking amplifier, which is biased in Class C and therefore remains off during low input-power operation. Before the signal reaches the peaking amplifier, a phase-compensation block introducing a 90° offset is employed. This phase adjustment is necessary to ensure that, when the peaking amplifier turns on, its output current is properly aligned with the carrier-path signal at the combining node. Thus, the phase-compensation network ensures constructive combination of the two branches at high input-power levels.

Both branches are connected at the load-modulation node, which also serves as the combining node. At low input levels, the peaking amplifier is inactive, and only the carrier amplifier delivers power to the load through the $\lambda/4$ impedance inverter. Under this condition, the carrier amplifier sees a transformed impedance that is higher than the nominal load, allowing it to maintain better efficiency in the output power back-off region. As the input power increases, the peaking amplifier begins to conduct and inject additional current into the combining node.

Once the peaking amplifier becomes active, the effective impedance seen by the carrier amplifier is dynamically modulated by the auxiliary current contribution. As a result, the carrier branch is gradually driven toward its optimum load condition as the output power approaches saturation. This active load-modulation mechanism

is the main reason for the improved efficiency of the Doherty amplifier compared with a conventional single-amplifier structure. Finally, the combined output power is delivered to the standard 50 Ω load, as indicated in Fig. 2.

The power splitter distributes the input signal to both branches, the carrier amplifier provides continuous amplification, the peaking amplifier supplies additional power only at high drive levels, the phase-compensation block maintains proper phase alignment, and the $\lambda/4$ impedance inverter enables the required load modulation. Through the coordinated action of these blocks, the final DPA achieves both high output power and improved efficiency at backed-off power levels.

2.2 Antenna Design and Simulation

The proposed transmitting antenna employs a dual-feed stacked microstrip patch configuration, as illustrated in Fig. 3. The antenna is realized using a three-layer substrate arrangement to improve the impedance bandwidth while maintaining a compact planar structure. The uppermost layer consists of a 0.8 mm-thick FR-4 substrate ($\varepsilon_r = 4.4$, $\tan\delta = 0.02$), on which a circular parasitic patch is printed, as shown in Fig. 3(a). The middle layer is designed using a 1.575 mm-thick Rogers RT/Duroid 5880 substrate ($\varepsilon_r = 2.2$, $\tan\delta = 0.0009$) and supports the square driven radiating patch. The third substrate, consisting of a 0.8 mm-thick Rogers RT/Duroid 5880 layer, is employed as the bottom layer to accommodate the feeding network. The optimized geometrical parameters of the transmitting antenna are summarized in Table 1.

As shown in Fig. 3(b), two independent 50-Ω microstrip transmission lines are printed on the bottom substrate to provide dual-feed excitation. The RF signals are transferred from the microstrip feed lines to the square driven patch through metallized via holes, thereby maintaining a completely planar feeding structure while reducing unwanted feed radiation. The dual-feed arrangement facilitates independent excitation of the transmitting antenna ports for subsequent integration with the DPA.

Table 1 Optimized Dimensions of the Dual-feed stacked patch transmitting antenna

Parameter	Dimension (mm)
L	86
W	86
l_1	27
w_1	27
r	15
f	33.25
f_1	4.8
G	8

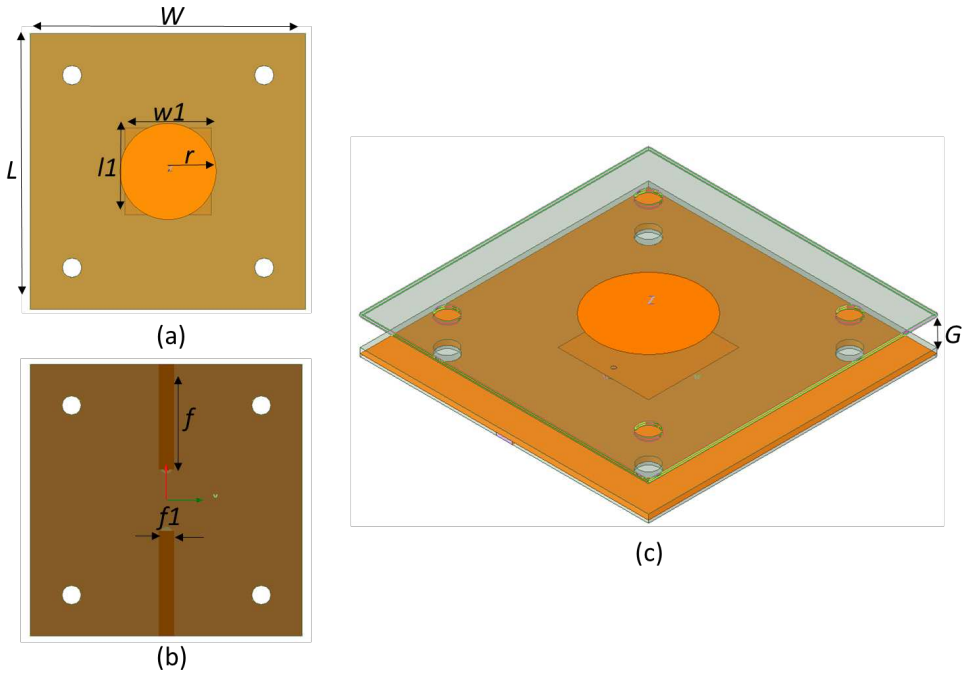

Fig. 3 Dual-feed stacked patch transmitting antenna: (a) Top view, (b) Bottom view, and (c) Isometric view.

The circular patch printed on the top substrate acts as a parasitic radiator, whereas the square patch printed on the middle substrate serves as the driven radiating element. An air gap of 8 mm is maintained between the upper parasitic patch and the lower driven patch, as illustrated in Fig. 3(c). The stacked configuration introduces electromagnetic coupling between the two radiating elements, resulting in multiple resonant modes that enhance the impedance bandwidth and improve the radiation performance.

A narrowband microstrip patch antenna was designed as the receiving antenna on a 1.575 mm-thick Rogers RT/Duroid 5880 substrate. The optimized geometric parameters are listed in Table 2, while the antenna configuration is illustrated in Fig. 4. The antenna employs a conventional coaxial probe feed and is designed to operate at the same resonant frequency as the transmitting antenna, thereby ensuring proper impedance matching and efficient wireless coupling. The receiving antenna is incorporated to receive the electromagnetic power radiated by the transmitting antenna and convert it into an electrical signal. As the radiated RF power cannot be directly evaluated after free-space propagation, the receiving antenna serves as the output load of the wireless link, enabling the evaluation of the received output power, transmission characteristics, and the overall performance of the proposed antenna-integrated DPA.

Table 2 Optimized Dimensions of the Receiving Antenna

Parameter	Dimension (mm)
L	40
W	40
l_1	25.5
w_1	25.5
Feed pin radius	0.0625
Coax inner radius	0.0625
Coax outer radius	2
Feed length	5

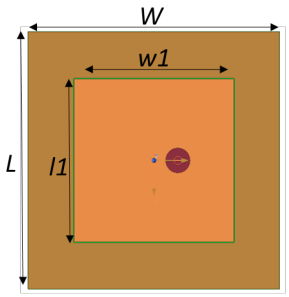

Fig. 4 Receiving antenna.

To evaluate the wireless transmission characteristics, both the transmitting and receiving antennas were incorporated into a single full-wave electromagnetic simulation model in Ansys HFSS. The simulation configuration is illustrated in Fig. 5. The antennas were positioned in a face-to-face arrangement with a separation distance of 20 cm, satisfying the far-field condition for the operating frequency. This configuration enables accurate evaluation of the transmission coefficient (S_{21}), received power, realized gain, and efficiency characteristics prior to the integration of the proposed DPA with the transmitting antenna.

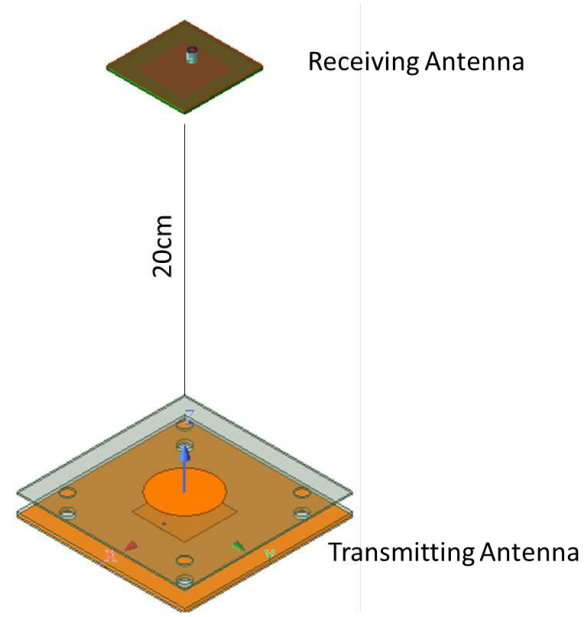

Fig. 5 Simulation model of the proposed dual-feed stacked patch transmitting antenna and receiving antenna.

2.3 Integration of Antenna with the Conventional DPA

Following the design of the conventional DPA, the proposed dual-feed stacked patch transmitting antenna was integrated directly at the output of the DPA, as shown in Fig. 6. In this configuration, the antenna acts as the radiating load of the amplifier, thereby eliminating the need for an additional output interface between the amplifier and the antenna.

The dual-feed stacked patch transmitting antenna consists of two independent feed ports. Port 1 is directly connected to the output of the DPA, i.e., the load modulation (combining) node, through which the amplified RF signal is delivered to the antenna for radiation. Port 2 is terminated with a matched 50-Ω load throughout the simulation. The matched termination minimizes reflections from the unused antenna port and preserves the desired impedance characteristics of the transmitting antenna during operation.

The receiving antenna captures the radiated electromagnetic field from the transmitting antenna, enabling the extraction of the transmission coefficient (S_{21}), received power, realized gain, and efficiency characteristics. The DPA–antenna integrated configuration is implemented and analyzed using Keysight ADS, providing an effective platform for evaluating the interaction between the power amplifier and the transmitting antenna while maintaining proper impedance matching at the unused antenna port.

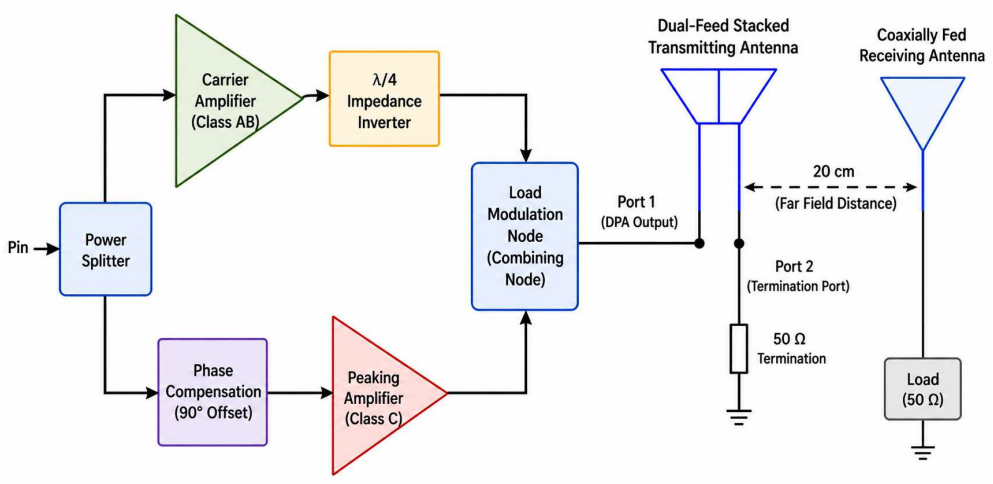

Fig. 6 Block diagram of the conventional DPA integrated with the antenna.

2.4 Transformer-Based Doherty Power Amplifier

To investigate an alternative output combining approach, the conventional load modulation (combining) node of the DPA is replaced with a 1:1 RF transformer, as illustrated in Fig. 7. In this configuration, the transformer functions as the output combining element by replacing the conventional combiner employed in the standard DPA architecture.

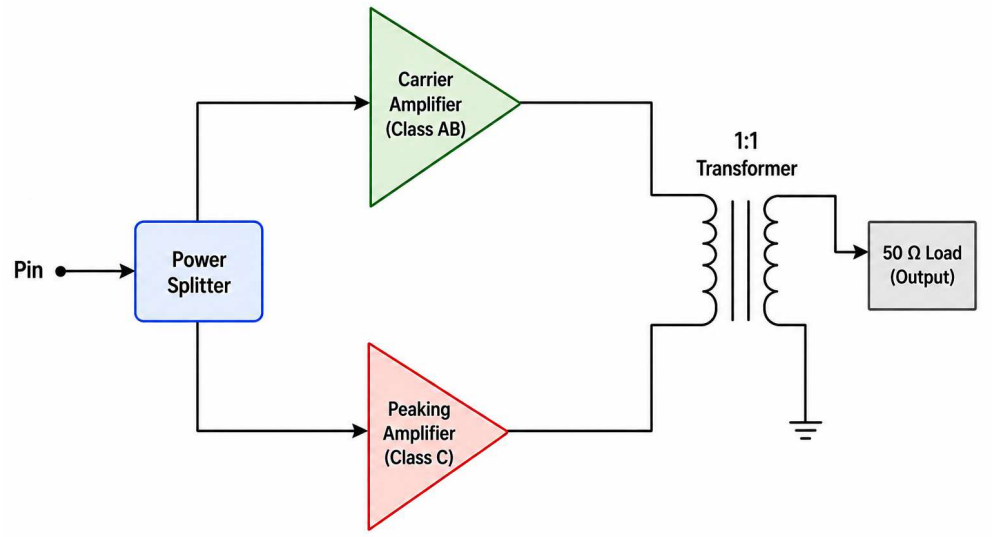

Fig. 7 Block diagram of the transformer-based DPA.

The output of the carrier amplifier is connected to the primary winding of the transformer, whereas the output of the peaking amplifier is connected directly to the opposite terminal of the primary winding. The transformer combines the RF signals generated by the carrier and peaking amplifier paths through magnetic coupling and transfers the combined power to the secondary winding. The secondary winding serves as the output interface of the transformer-based DPA. One terminal of the secondary winding is connected to a matched 50-Ω load, while the other terminal is connected to ground, thereby providing the required output termination for evaluating the amplifier performance.

2.5 Antenna Combined Doherty Power Amplifier

Following the transformer-based DPA architecture, the 1:1 RF transformer is replaced by the proposed dual-feed stacked patch transmitting antenna, as illustrated in Fig. 8. In the proposed configuration, the transmitting antenna performs the dual function of radiating the amplified RF signal while simultaneously acting as the output combining element of the DPA.

The proposed transmitting antenna consists of two independent feed ports. Feed 1 is connected to the output of the carrier amplifier through the $\lambda/4$ impedance inverter, whereas Feed 2 is directly connected to the output of the peaking amplifier. Unlike the conventional DPA, where the carrier and peaking amplifier outputs are combined using an output combiner or a transformer, the proposed architecture directly excites the two feed ports of the transmitting antenna. Consequently, the antenna serves as the radiating element while eliminating the requirement for an additional output combining network.

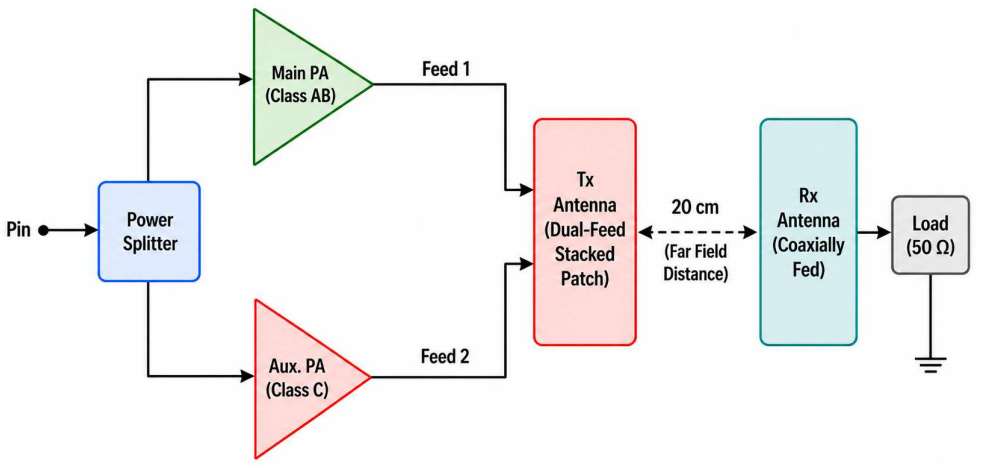

Fig. 8 Block diagram of the proposed DPA–antenna integrated architecture.

Since the transmitting antenna is directly integrated with the DPA output, the proposed configuration reduces the number of passive components in the output stage and provides a compact amplifier–antenna integrated architecture.

3 Results and Discussion

3.1 Conventional Doherty Power Amplifier

The small- and large-signal performances of the conventional DPA were first investigated to establish a reference for evaluating the proposed antenna-integrated architecture. The amplifier was designed at the center frequency of 3.7 GHz using a Class-AB carrier amplifier and a Class-C peaking amplifier based on the conventional Doherty load-modulation principle.

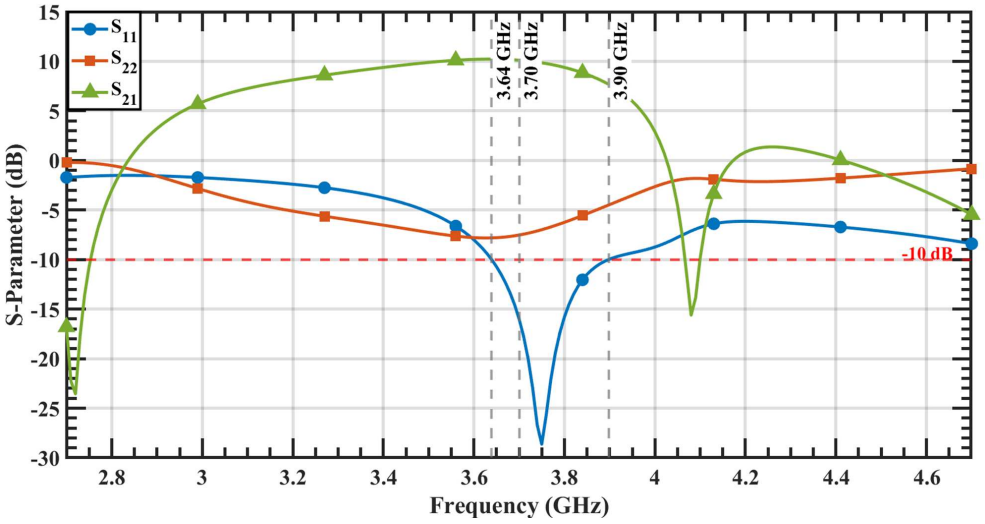

Fig. 9 S-parameter of the conventional DPA

Fig. 9 presents the simulated small-signal S-parameter characteristics. The input reflection coefficient (S_{11}) reaches a minimum of -28 dB at 3.75 GHz, with a -10 dB impedance bandwidth from 3.64 GHz to 3.90 GHz, corresponding to 260 MHz. The forward transmission coefficient (S_{21}) reaches 10.1 dB at the operating frequency, while S_{22} attains a minimum of approximately -8 dB near the design frequency. Although the output return loss does not reach -10 dB, this is acceptable since the output network is primarily optimized for large-signal load modulation rather than small-signal output matching. These results confirm satisfactory impedance transformation for subsequent nonlinear operation.

The large-signal performance as a function of source power is shown in Fig. 10.

At low excitation levels, only the carrier amplifier is active, resulting in relatively low DE and PAE. With increasing source power, the peaking amplifier turns on and contributes additional current to the combining node, producing the expected load-modulation behavior. Consequently, DE and PAE increase significantly beyond 20 dBm. The maximum DE reaches 72% at 36 dBm, while the peak PAE is 62%

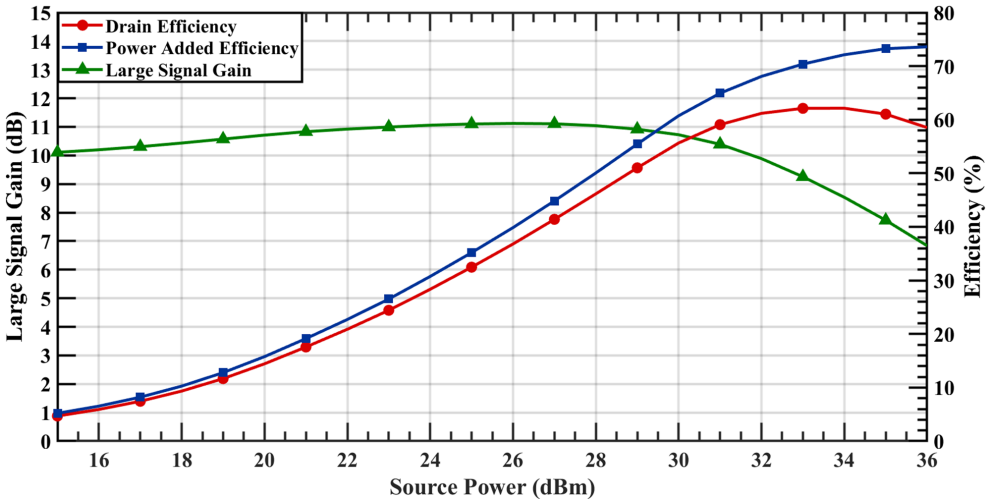

Fig. 10 Drain efficiency, power added efficiency and large signal gain of the conventional DPA versus source power

near 34 dBm. At higher drive levels, the PAE decreases as the amplifier approaches saturation, followed by a gradual reduction in DE.

The large-signal gain remains close to 10 dB over the low- and medium-power regions and reaches approximately 11.2 dB before compression. Near saturation, the gain gradually decreases due to the nonlinear behavior of the active devices. Nevertheless, the relatively stable gain over the useful operating range indicates proper interaction between the carrier and peaking branches.

Fig. 11 shows the variation of DE, PAE, and large-signal gain with output power. The output power increases with source power and reaches a saturated value of approximately 43 dBm.saturated output power of 43 dBm.

The corresponding DE increases with output power and reaches 72%, while the maximum PAE is 62%. The large-signal gain remains around 11 dB throughout the main operating region and decreases only near saturation because of gain compression. These characteristics establish the conventional DPA as a suitable reference architecture for evaluating the subsequent antenna-integrated configuration.

3.2 Performance of the Transmitting and Receiving Antennas

The simulated performance of the proposed transmitting and receiving antennas was evaluated in terms of impedance matching and radiation characteristics. The reflection coefficients of both antennas are first presented in Fig. 12 to verify proper impedance matching over the operating frequency band. Subsequently, the realized gain patterns of the transmitting and receiving antennas in the principal planes are illustrated in Figs. 13 and 14, respectively, to demonstrate their radiation performance.

From Fig. 12, it can be observed that the transmitting antenna exhibits a wide impedance bandwidth, with both S_{11} and S_{22} remaining below the conventional

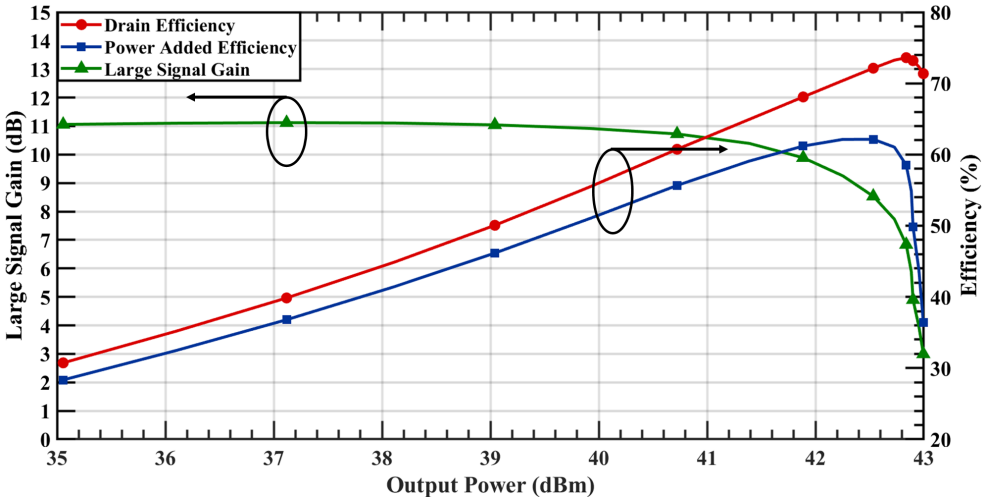

Fig. 11 Drain efficiency, power added efficiency and large signal gain of the conventional DPA versus output power

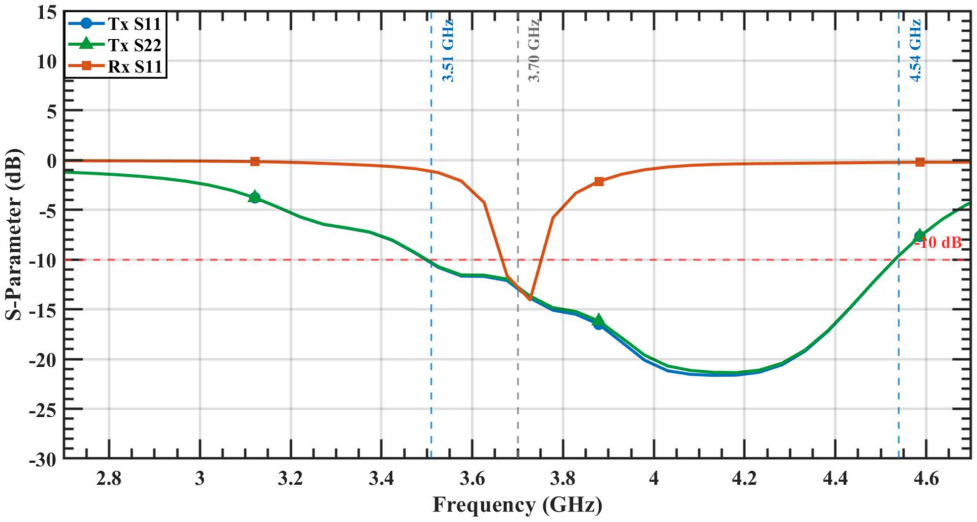

Fig. 12 S-prameter of the transmitting and Receiving antenna

−10 dB criterion from 3.51 GHz to 4.54 GHz. The two reflection coefficients show closely similar responses over the operating band, indicating consistent impedance matching at the two transmitting ports. At the DPA center frequency of 3.7 GHz, both S_{11} and S_{22} are approximately −13 dB, confirming impedance matching at the intended operating frequency. Although the minimum reflection coefficients of the

transmitting ports are slightly frequency-shifted from the DPA center frequency, the wide impedance bandwidth ensures stable operation over the required frequency range.

In contrast, the receiving antenna exhibits a relatively narrowband response centered around the DPA operating frequency. At 3.7 GHz, the receiving antenna also provides a reflection coefficient of −13 dB, indicating good impedance matching at the desired operating frequency and enabling efficient power reception. Therefore, the proposed antenna pair provides complementary impedance characteristics, with the transmitting antenna offering wideband operation through its two ports and the receiving antenna being selectively tuned around the 3.7-GHz DPA center frequency. These characteristics make the antenna pair suitable for direct integration with the proposed DPA and for reliable wireless power transfer between the transmitting and receiving antennas.

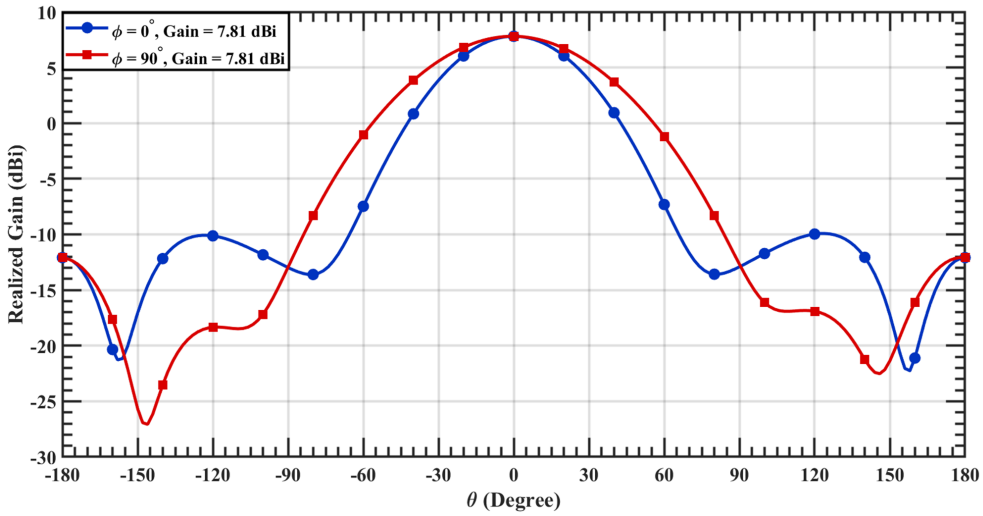

Fig. 13 Realized gain of the transmitting antenna

Fig. 13 illustrates the realized gain patterns of the proposed dual-feed stacked transmitting antenna in the principal planes ($\phi = 0°$ and $\phi = 90°$). The antenna exhibits a broadside radiation pattern with a maximum realized gain of 7.81 dBi in both planes, indicating nearly symmetrical radiation characteristics. The radiation patterns are dominated by a strong main lobe directed along the boresight, while the side and back lobes remain significantly lower than the main beam. Minor differences observed at larger observation angles are mainly attributed to the dual-feed excitation and the finite ground plane. Overall, the transmitting antenna provides stable directional radiation with sufficient gain for efficient wireless power transmission.

The realized gain patterns of the coaxially fed receiving antenna are shown in Fig. 14. Similar to the transmitting antenna, the receiving antenna exhibits broadside radiation with a maximum realized gain of 7.14 dBi in both the $\phi = 0°$ and

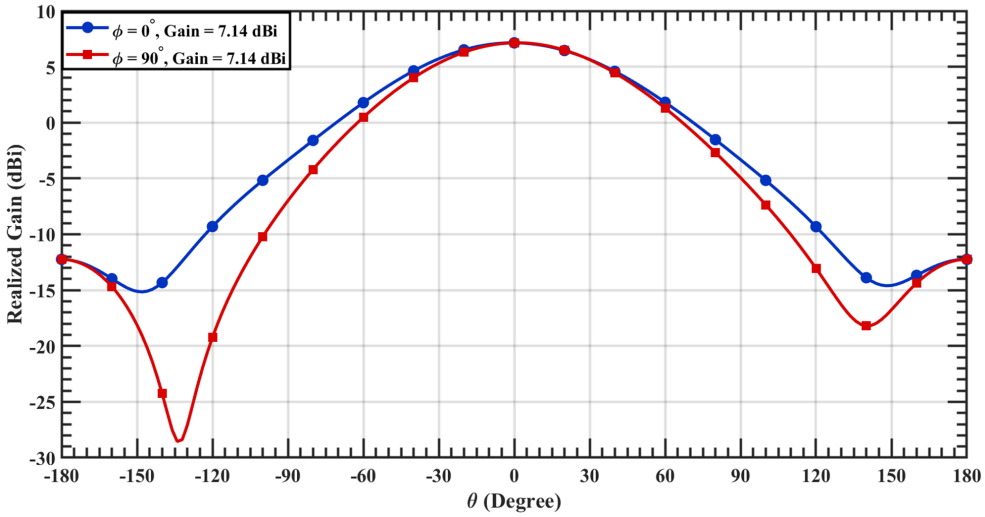

Fig. 14 Realized gain of the receiving antenna

$\phi = 90°$ planes, demonstrating nearly identical radiation characteristics in the two orthogonal planes. The radiation patterns remain smooth and symmetric about the boresight direction, indicating stable directional performance and efficient reception of electromagnetic energy transmitted by the proposed transmitting antenna.

The simulated impedance matching and realized gain results demonstrate that both antennas are well suited for operation at the target frequency of 3.7 GHz. The transmitting antenna provides wide impedance bandwidth together with stable directional radiation, while the receiving antenna offers excellent impedance matching and consistent broadside gain. These characteristics make the antenna pair well suited for integration with the DPA architecture and subsequent far-field wireless power transmission analysis.

3.3 Integration of the Antenna with the Conventional Doherty Power Amplifier

Figure 15 presents the simulated small-signal S-parameter characteristics of the conventional DPA with the transmitting antenna connected at its output. Compared with the standalone DPA, the input impedance bandwidth increases from 260 MHz to 320 MHz, while the minimum S_{11} reaches -22 dB. This bandwidth enhancement is attributed to the impedance characteristics of the dual-feed stacked antenna, which provides a broader matching response than a conventional 50-Ω load.

The output reflection coefficient, S_{22}, exhibits a resonance near 3.7 GHz, reaching -13 dB, corresponding to the resonant response of the antenna configuration. The relatively low S_{21} near the operating frequency results from evaluating the complete transmitting–receiving antenna configuration, where antenna coupling and the

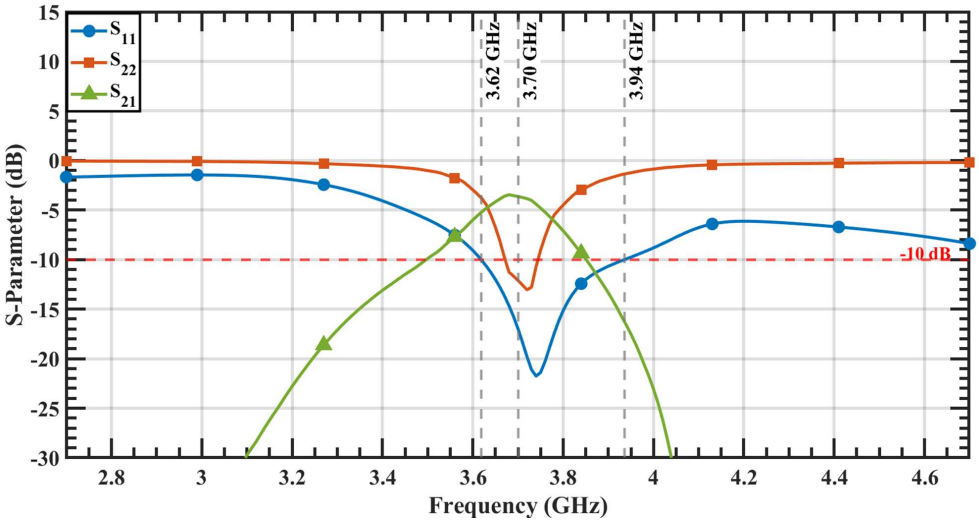

Fig. 15 S-parameter of the conventional DPA with antenna

receiving-antenna response contribute to the measured transmission. Therefore, S_{21} does not directly represent the intrinsic small-signal gain of the DPA.

The large-signal characteristics with respect to source power are shown in Fig. 16. The DE, PAE, and large-signal gain retain trends similar to those of the standalone DPA, confirming that the Doherty load-modulation mechanism is preserved after antenna integration. The peak DE decreases to 68%, while the peak PAE decreases from 62% to 59%. This reduction is mainly attributed to the additional losses and impedance variation introduced by the antenna, which shift the amplifier from its optimum load condition. In contrast, the large-signal gain increases slightly to approximately 11.5 dB and remains relatively stable before gain compression, indicating limited impact of the antenna loading on the gain characteristics.

The corresponding output-power characteristics are presented in Fig. 17. The amplifier achieves a saturated output power of 43 dBm, which is comparable to the standalone DPA. The large-signal gain remains around 11.5 dB over the main operating region, while the reduced DE and PAE reflect the nonideal impedance and losses introduced by the antenna.

These results indicate that replacing the conventional 50-Ω load with the transmitting antenna preserves the fundamental operating characteristics of the Doherty amplifier, while the slight reduction in efficiency arises from the practical impedance presented by the antenna rather than an ideal matched load.

3.4 Transformer-Based Doherty Power Amplifier

To investigate replacing the conventional output combining network with the transmitting antenna, a transformer-based Doherty power amplifier (DPA) was first designed.

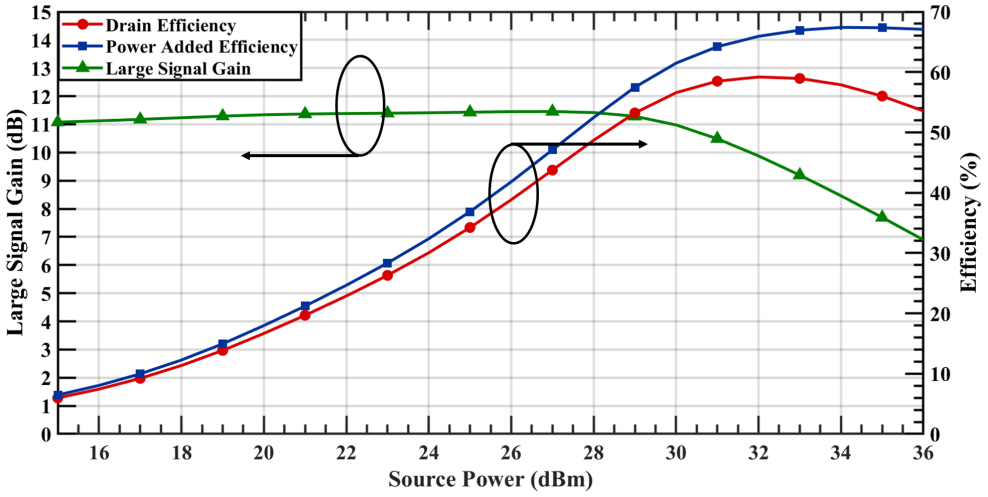

Fig. 16 Drain efficiency, power added efficiency and large signal gain of the conventional DPA with antenna versus source power

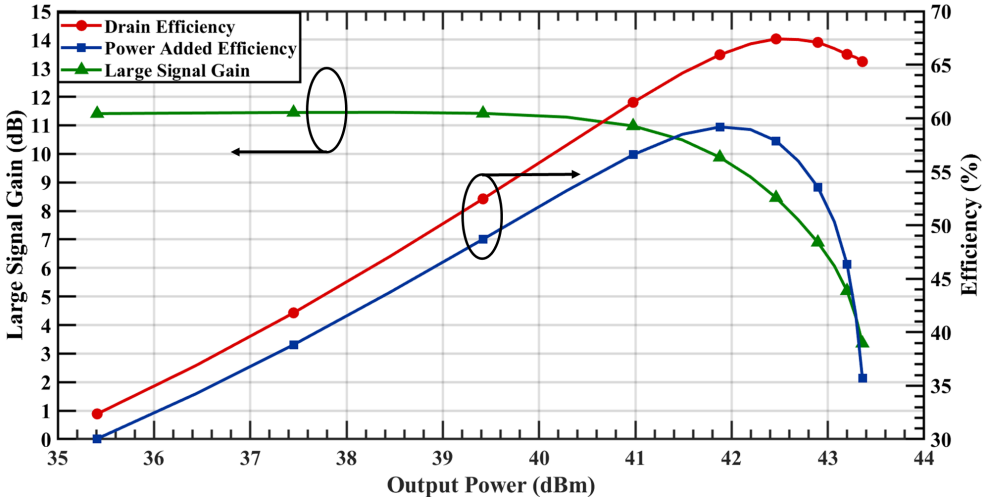

Fig. 17 Drain efficiency, power added efficiency and large signal gain of the conventional DPA with antenna versus output power

The transformer provides an intermediate combining network to validate the Doherty load-modulation mechanism before antenna integration.

Fig. 18 shows the simulated S-parameters, where the transformer-based DPA provides improved input matching and wider impedance bandwidth while maintaining comparable forward gain.

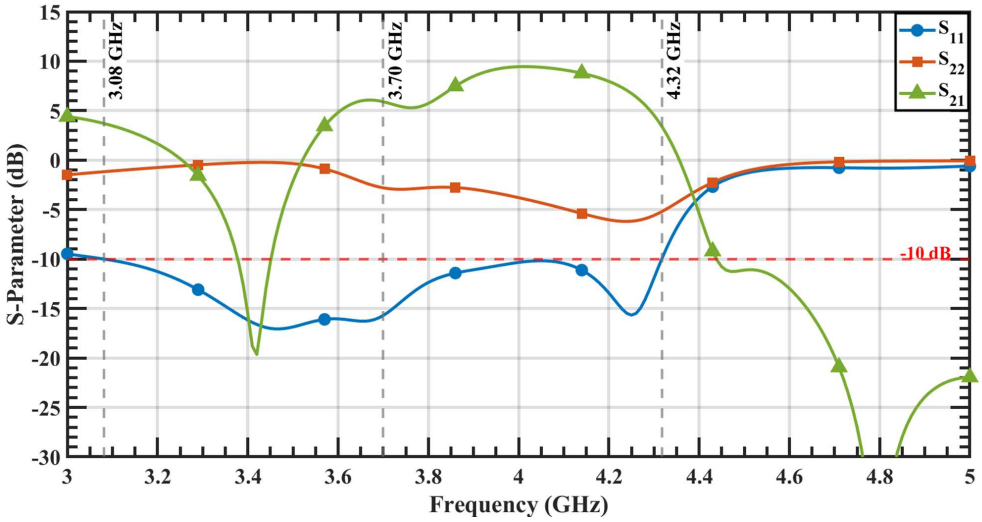

Fig. 18 S-parameter of the transformer based DPA

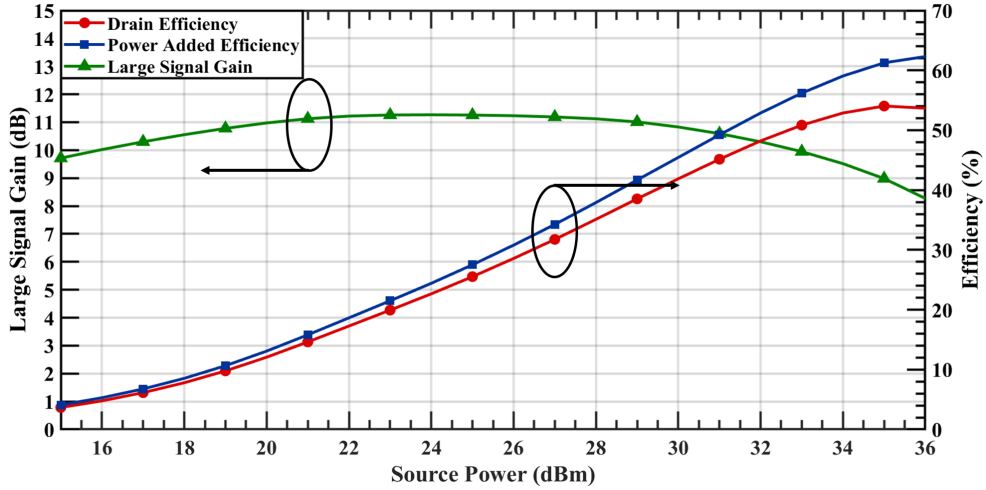

Fig. 19 Drain efficiency, power added eficiency and large signal gain of the transformer based DPA versus source power

The large-signal characteristics in Fig. 19 and Fig. 20 demonstrate the expected Doherty behavior, with increasing efficiency due to peaking-amplifier activation and nearly constant large-signal gain before compression.

These results demonstrate that the transformer can replace the conventional quarter-wave impedance inverter while preserving DPA operation, providing an

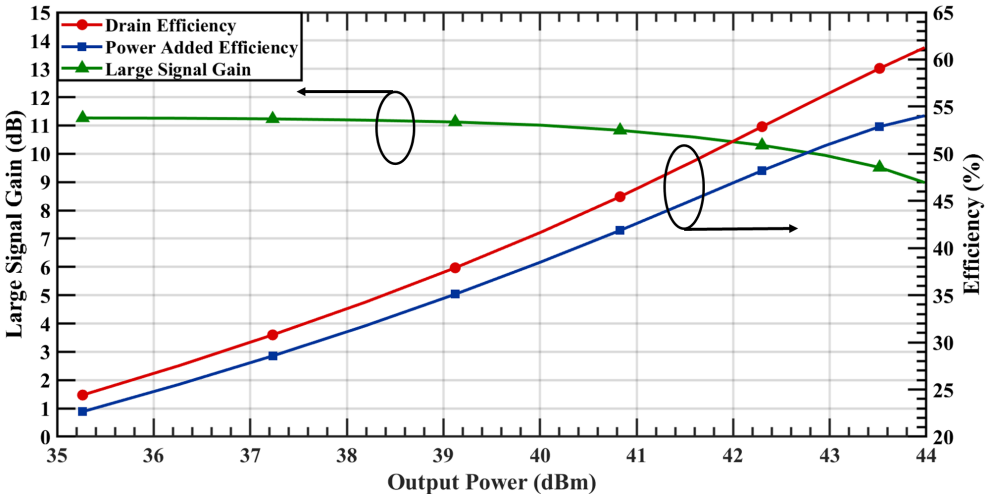

Fig. 20 Drain efficiency, power added eficiency and large signal gain of the transformer based DPA versus output power

intermediate validation step for the proposed antenna-integrated output combining network.

3.5 Proposed Antenna-Integrated Doherty Power Amplifier

Following the successful verification of the transformer-based DPA, the transformer output combining network was replaced by the proposed dual-feed transmitting antenna to realize the antenna-combined DPA. In this configuration, the antenna simultaneously performs the functions of power combining and radiation, thereby eliminating the conventional passive combining network while preserving the Doherty load-modulation mechanism.

Fig. 21 presents the simulated S-parameter characteristics of the proposed antenna-combined DPA.

The input reflection coefficient (S_{11}) exhibits a deep resonance of approximately -41 dB at 3.82 GHz, indicating excellent input impedance matching. The -10 dB impedance bandwidth extends from 3.20 GHz to 4.31 GHz, corresponding to a wide bandwidth of about 1.11 GHz. This broad matching response demonstrates that the antenna-integrated output network maintains satisfactory input matching over a wide frequency range.

The output reflection coefficient (S_{22}) exhibits a narrow resonant response around the 3.7 GHz operating frequency, with a minimum value of -14 dB. This narrowband behavior is mainly attributed to the receiving (Rx) antenna, which was designed for narrowband operation at the target frequency. Consequently, the S_{22} response is dominated by the resonant characteristics of the Rx antenna rather than the broadband input matching behavior of the DPA. The forward transmission coefficient (S_{21}) reaches -5.5 dB at 3.7 GHz and decreases away from the resonant region. Since

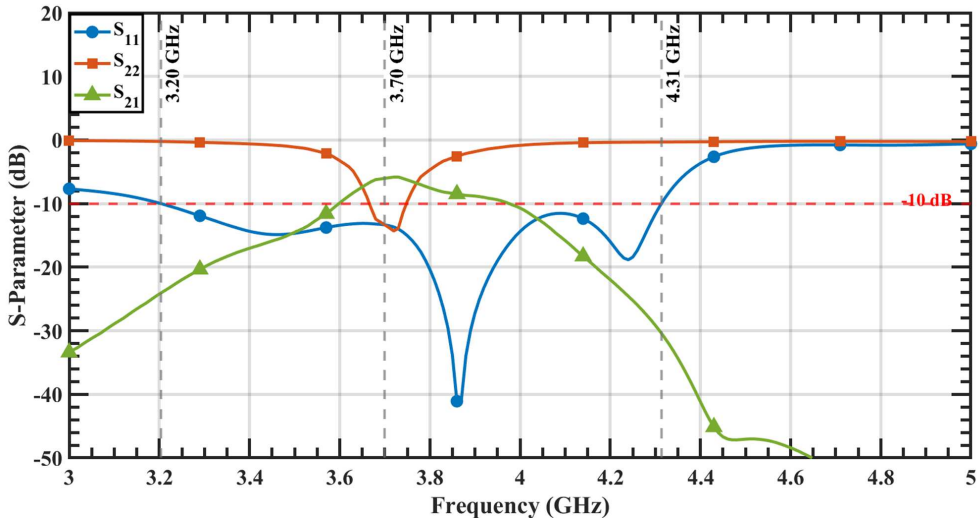

Fig. 21 S-parameter of the antenna combined DPA

the simulated configuration includes both transmitting and receiving antennas, the obtained S_{21} reflects the overall frequency-dependent transmission characteristics of the integrated wireless link and therefore does not directly represent the intrinsic gain of the DPA. Overall, the results confirm excellent input matching over a wide bandwidth, together with the expected narrowband output response imposed by the Rx antenna.

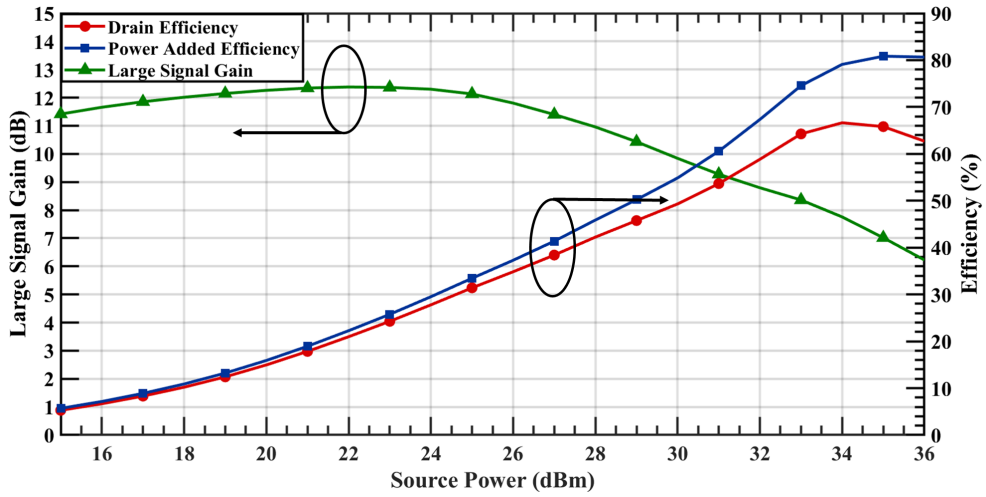

Fig. 22 Drain efficiency, power added efficiency and large signal gain of the antenna combined DPA versus source power

The large-signal characteristics with respect to source power are shown in Fig. 22. Similar to the transformer-based DPA, the proposed architecture exhibits the characteristic Doherty operation, where the drain efficiency (DE) and power-added efficiency (PAE) increase rapidly after the peaking amplifier becomes active. However, compared with the transformer-based DPA, the proposed design achieves a peak drain efficiency of approximately 80%, whereas the transformer-based DPA reaches about 63%. Likewise, the peak PAE increases from approximately 60% to about 67%, while the large-signal gain improves from approximately 11.3 dB to about 12.4 dB. These results demonstrate that replacing the transformer with the transmitting antenna not only preserves the Doherty load-modulation mechanism but also enhances the RF performance by reducing the losses associated with the conventional output combining network.

Fig. 23 illustrates the corresponding large-signal characteristics with respect to output power.

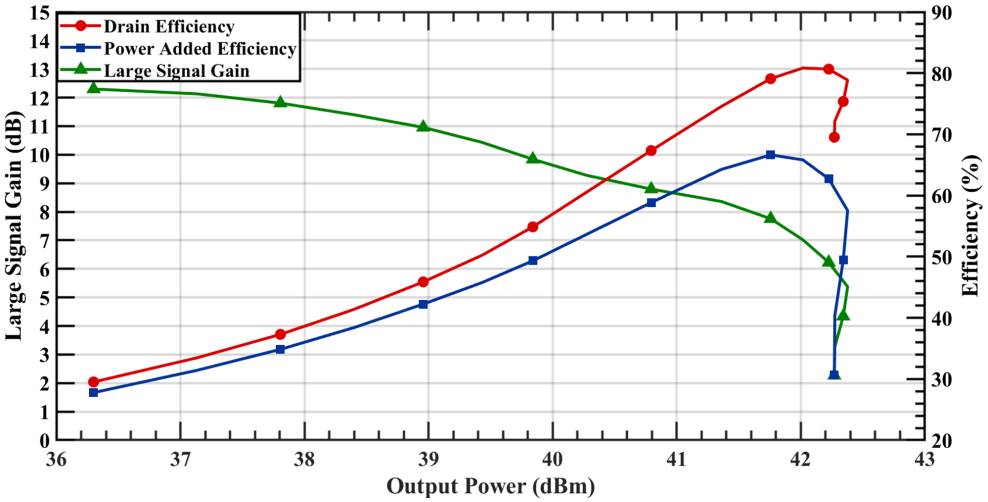

Fig. 23 Drain efficiency, power added efficiency and large signal gain of the antenna combined DPA versus output power

The proposed antenna-combined DPA maintains a saturated output power of approximately 42 dBm, which is comparable to that of the transformer-based DPA. In addition, the drain efficiency reaches approximately 80%, while the peak PAE approaches 67%. The large-signal gain remains above 12 dB over most of the operating region before gradually decreasing near saturation because of gain compression. Compared with the transformer-based DPA, the proposed architecture provides approximately 17 percentage points higher drain efficiency, about 7 percentage points higher PAE, and nearly 1 dB improvement in large-signal gain without sacrificing the output power capability.

Overall, the proposed antenna-combined DPA successfully demonstrates that the dual-feed transmitting antenna can effectively replace the transformer-based output combining network while maintaining the desired Doherty operation. The proposed architecture preserves the wide operating bandwidth and output power capability while simultaneously improving the gain and efficiency. These results validate the proposed concept of employing the transmitting antenna as both the radiating element and the output power combiner, thereby simplifying the output network and enhancing the overall performance of the Doherty power amplifier.

3.6 Comparison of the Conventional Doherty power Amplifier and Antenna integrated Doherty Power Amplifiers

The large-signal characteristics as a function of source power are illustrated in Fig. 24. Compared with the conventional DPA with antenna, the proposed antenna-combined DPA achieves a higher peak drain efficiency of approximately 80%, whereas the conventional architecture reaches about 67%. Similarly, the peak power-added efficiency increases from approximately 59% to about 67%, and the large-signal gain improves by nearly 1 dB around the optimum operating region. However, at lower input power levels (below approximately 28–30 dBm), the conventional DPA with antenna exhibits slightly higher drain efficiency and power-added efficiency.

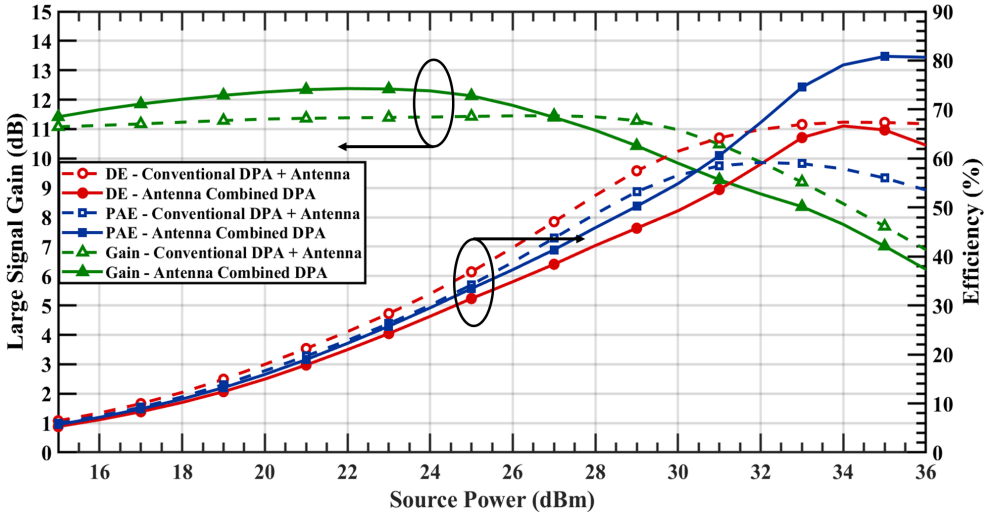

Fig. 24 Drain efficiency, power added efficiency and large signal gain of the conventional DPA with antenna and antenna combined DPA versus source power

Furthermore, the gain of the proposed antenna-combined DPA begins to compress at a lower input power than the conventional architecture, resulting in a narrower high-gain operating region before saturation.

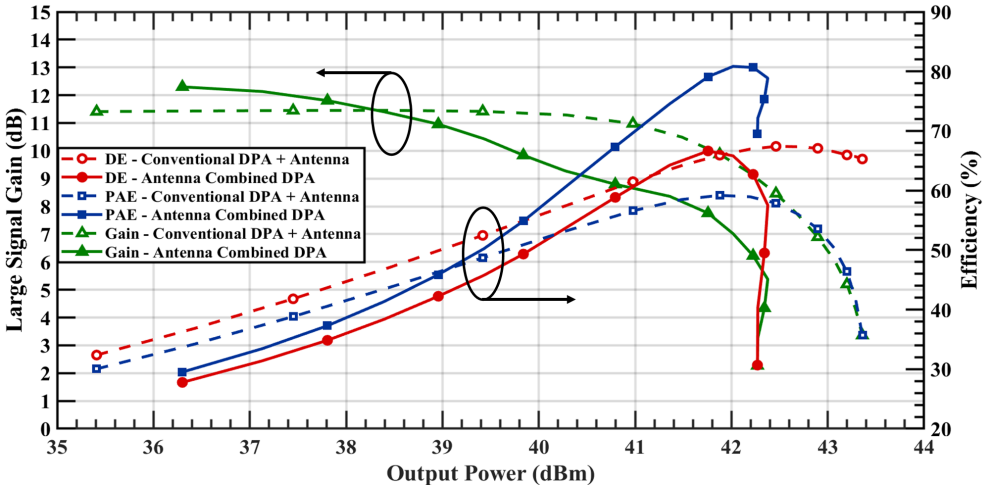

Fig. 25 Drain efficiency, power added efficiency and large signal gain of the conventional DPA with antenna and antenna combined DPA versus output power

A comparison of the large-signal performance with respect to output power is provided in Fig. 25. Both architectures achieve nearly the same saturated output power of approximately 42 dBm, confirming that replacing the conventional output combining network with the transmitting antenna does not alter the maximum output power capability. The proposed antenna-combined DPA consistently provides higher drain efficiency and power-added efficiency over the medium- and high-output-power regions. Nevertheless, the large-signal gain decreases more rapidly after the onset of gain compression, whereas the conventional DPA with antenna maintains a relatively stable gain over a slightly wider output power range. Therefore, the proposed architecture achieves enhanced efficiency while maintaining the characteristic Doherty operation and saturated output power, although the high-gain operating region is comparatively narrower.

The output power characteristics of both architectures are further evaluated as a function of source power, as shown in Fig. 26.

Nearly identical output power responses are observed throughout the operating range, with both amplifiers reaching saturation at 42 dBm. The proposed antenna-combined DPA exhibits a slightly higher output power over the low- and medium-input-power regions, while the difference becomes negligible near saturation. These results indicate that replacing the conventional output combining network with the transmitting antenna preserves the output power capability, and that the performance enhancement is primarily reflected in the improved gain and efficiency characteristics rather than an increase in maximum output power.

Table 3 summarizes the key performance parameters of all the investigated DPA architectures.

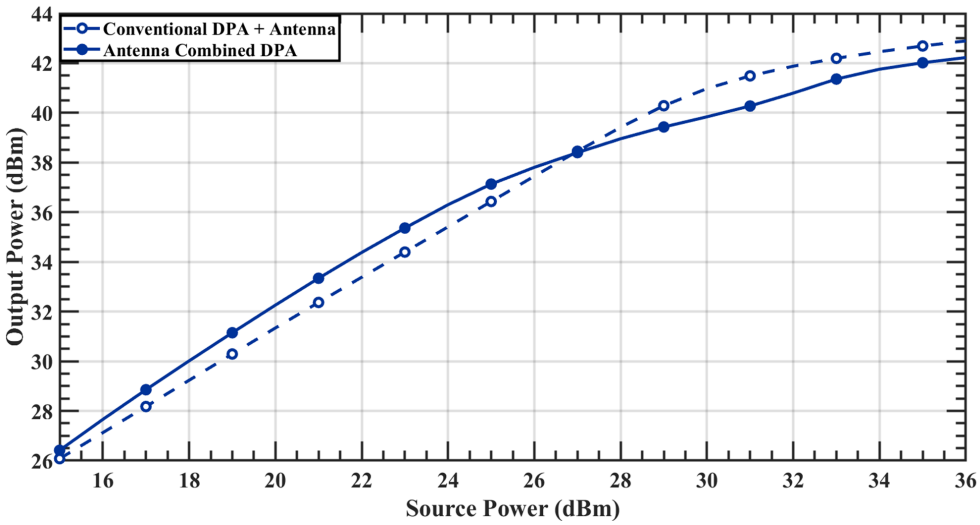

Fig. 26 output power of the conventional DPA with antenna and antenna combined DPA versus source power

Table 3 Performance Comparison of Different DPA Architectures

Parameter	Conventional DPA	Conventional DPA with Antenna	Transformer-Based DPA	Proposed Antenna-Combined DPA
Impedance Bandwidth (MHz)	260	320	1110	1110
Peak Large-Signal Gain (dB)	11.2	11.5	11.3	12.4
Peak Drain Efficiency (%)	72	68	63	80
Peak Power-Added Efficiency (%)	62	59	60	67
Saturated Output Power (dBm)	43	43	42.2	42.2

It is evident that the proposed antenna-combined DPA achieves the highest drain efficiency, power-added efficiency, and large-signal gain while maintaining a comparable saturated output power. In addition, the proposed architecture significantly enhances the impedance bandwidth from 260 MHz in the conventional DPA to 1.11 GHz, demonstrating the effectiveness of employing the dual-feed transmitting antenna as both the electromagnetic power-combining network and the radiating element while preserving the characteristic Doherty load-modulation operation.

4 CONCLUSION

An antenna-integrated Doherty power amplifier operating at 3.7 GHz has been presented and investigated, where the antenna element acts as Doherty combiner. The proposed architecture employs a dual-feed stacked-patch transmitting antenna that is directly connected to the carrier and peaking amplifier branches, allowing the antenna to perform electromagnetic power combining and radiation simultaneously. The proposed antenna-combined DPA achieves an impedance bandwidth of 1.11 GHz, compared with 320 MHz for the conventional DPA with antenna. In addition, a peak large-signal gain of 12.4 dB, peak drain efficiency of approximately 80%, peak power-added efficiency of 67%, and saturated output power of 42.2 dBm are obtained. The comparison with the transformer-based DPA confirms that the transmitting antenna can effectively replace the conventional output-combining network while preserving the characteristic Doherty load-modulation. These results demonstrate the feasibility of using the transmitting antenna as an integral part of the DPA output stage for compact and broadband RF transmitter architectures. This will also enable integration in active antenna arrays for high EIRP applications like Macro Base stations and RADAR.

The comparison with conventional DPA with an antenna also highlights important design trade-offs. Although the proposed antenna-combined DPA provides higher drain efficiency and power-added efficiency in the medium- and high-power regions, its efficiency is slightly lower at low input-power levels. Furthermore, the proposed architecture exhibits gain compression at a lower input power level and a comparatively narrower high-gain operating region, while maintaining a nearly unchanged saturated output power of approximately 42 dBm. Therefore, the proposed architecture achieves the primary objectives of eliminating the separate output-combining network and substantially enhancing the impedance bandwidth, while maintaining the fundamental Doherty operation and comparable output-power capability. Further optimization of the antenna feeds, branch impedances, mutual coupling, and phase relationship between the carrier and peaking paths can be considered to improve these trade-offs.

The present implementation employs a single-polarized transmitting antenna. As a continuation of the work in future, the proposed architecture can be integrated to a dual-polarized antenna configuration to support polarization diversity and more flexible wireless transmission. Furthermore, the single antenna element can be extended to an antenna array to obtain high EIRP, beam steering, and improved spatial coverage. With these extensions, the antenna-combined DPA concept can be explored for compact and broadband transmitter front ends targeting applications such as 5G FR1 wireless communication, broadband wireless systems, and satellite communication systems. The broader relevance of these application areas is consistent with the increasing demand for high-efficiency and broadband RF transmitters.

References

[1] Y. Xu, J. Pang, X. Wang, and A. Zhu, "Enhancing bandwidth and back-off range of Doherty power amplifier with modified load modulation network," *IEEE Transactions on Microwave Theory and Techniques*, vol. 70, no. 1, pp. 210–221, 2022,

doi: 10.1109/TMTT.2021.3056402.

[2] X. Y. Zhou, W. S. Chan, W. Feng, X. Fang, T. Sharma, and S. Chen, "Broadband Doherty power amplifier based on coupled phase compensation network," *IEEE Transactions on Microwave Theory and Techniques*, vol. 70, no. 1, pp. 210–221, 2022, doi: 10.1109/TMTT.2021.3057628.

[3] H. Chen, J.-X. Xu, and X. Y. Zhang, "Miniaturized broadband Doherty power amplifier using simplified output matching topology," *IEEE Transactions on Circuits and Systems I: Regular Papers*, vol. 69, no. 8, 2022, doi: 10.1109/TCSI.2022.3169883.

[4] C. F. Gonçalves *et al.*, "Quasi-load insensitive Doherty power amplifier using supply voltage and input excitation adaptation," *IEEE Transactions on Microwave Theory and Techniques*, 2022, doi: 10.1109/TMTT.2021.3112168.

[5] A. Piacibello, V. Camarchia, P. Colantonio, and R. Giofrè, "3-way Doherty power amplifiers: Design guidelines and MMIC implementation at 28 GHz," *IEEE Transactions on Microwave Theory and Techniques*, 2023, doi: 10.1109/TMTT.2022.3225316.

[6] H. Lyu, K. Chen *et al.*, "Analysis and design of reconfigurable multiband mismatch-resilient quasi-balanced Doherty power amplifier for massive MIMO systems," *IEEE Transactions on Microwave Theory and Techniques*, 2023, doi: 10.1109/TMTT.2022.3198437.

[7] A. Piacibello *et al.*, "A 5-W GaN Doherty amplifier for Ka-band satellite downlink with 4-GHz bandwidth and 17-dB NPR," *IEEE Microwave and Wireless Components Letters*, vol. 32, no. 8, pp. 964–967, 2022, doi: 10.1109/LMWC.2022.3160227.

[8] J. Shin *et al.*, "Broadband virtual-stub Doherty power amplifier using asymmetric structure," *IEEE Access*, vol. 11, pp. 101425–101434, 2023, doi: 10.1109/ACCESS.2023.3315608.

[9] Y. Chen *et al.*, "New compact load network for Doherty power amplifiers based on L-section matching network of the carrier amplifier and post-matching network," *IEEE Access*, vol. 11, pp. 66478–66487, 2023, doi: 10.1109/ACCESS.2023.3291219.

[10] X. Zhang, S. Li, and T. Chi, "A millimeter-wave watt-level Doherty power amplifier in silicon," *IEEE Transactions on Microwave Theory and Techniques*, vol. 72, no. 3, pp. 1674–1686, 2024, doi: 10.1109/TMTT.2023.3311954.

[11] H. Oh *et al.*, "A multimode GaN Doherty power amplifier MMIC with N-scalable amplifiers for selective back-off power level," *IEEE Transactions on Microwave Theory and Techniques*, vol. 72, no. 1, pp. 550–562, 2024, doi:

10.1109/TMTT.2023.3316356.

[12] L. Zhou, X. Zhou, and W. S. Chan, "Compact dual-passband Doherty power amplifier based on stub-loaded stepped-impedance transformer," *IEEE Transactions on Circuits and Systems I: Regular Papers*, vol. 71, no. 1, pp. 99–109, 2024, doi: 10.1109/TCSI.2023.3323457.

[13] F. Dietrich, M.-D. Wei, E. Heidebrecht, D. Bierbüsse, and R. Negra, "Load and frequency independent Doherty power amplifier back-off extension," *IEEE Transactions on Microwave Theory and Techniques*, vol. 72, no. 6, pp. 3438–3451, 2024, doi: 10.1109/TMTT.2023.3335620.

[14] Z. Dai *et al.*, "Design of wideband asymmetric Doherty power amplifier using a new phase compensation technique," *IEEE Transactions on Circuits and Systems I: Regular Papers*, vol. 71, no. 3, pp. 1093–1104, 2024, doi: 10.1109/TCSI.2023.3336558.

[15] J. Guo *et al.*, "An ultra-broadband load-insensitive dual-input Doherty power amplifier MMIC using configurable supply voltage for 5G smartphones," *IEEE Transactions on Microwave Theory and Techniques*, vol. 73, no. 6, pp. 3514–3528, 2025, doi: 10.1109/TMTT.2024.3501312.

[16] K. Liu *et al.*, "Symmetrical Doherty power amplifier with extended bandwidth and back-off range based on nonlinear current profile," *IEEE Transactions on Circuits and Systems I: Regular Papers*, vol. 72, no. 7, pp. 3204–3214, 2025.

[17] B. H. Zeng, Y. F. Pan, F. C. Yuan, W. S. Chan, and S. Y. Zheng, "Input phase controlled Doherty power amplifier with out-phased current load modulation for arbitrary output back-off," *IEEE Transactions on Circuits and Systems I: Regular Papers*, vol. 72, no. 6, pp. 2626–2638, 2025, doi: 10.1109/TCSI.2025.3557496.

[18] S. Liu *et al.*, "Highly-efficient broadband GaAs HBT Doherty power amplifier with harmonic control technique for 5G application," *IEEE Transactions on Circuits and Systems II: Express Briefs*, vol. 72, no. 5, pp. 713–717, 2025.

[19] S. Liu, Y. Zhang, J. Pang, R. Gao *et al.*, "Analysis and design of ultrawideband generalized asymmetrical Doherty power amplifier using hybrid voltage–current configuration," *IEEE Transactions on Microwave Theory and Techniques*, vol. 73, no. 10, pp. 8247–8257, 2025, doi: 10.1109/TMTT.2025.3568462.

[20] Y. Zhang, J. Pang, R. Gao, M. Li *et al.*, "Dual-wideband three-stage Doherty power amplifier using reciprocal bias configuration," *IEEE Transactions on Microwave Theory and Techniques*, vol. 73, no. 9, pp. 6209–6220, 2025, doi: 10.1109/TMTT.2025.3551738.

[21] R. Gao *et al.*, "Broadband GaAs HBT Doherty power amplifier using lumped compensation network and input phase correction for 5G applications," *IEEE*

Transactions on Circuits and Systems I: Regular Papers, vol. 73, no. 4, pp. 2510–2521, 2026, doi: 10.1109/TCSI.2025.3619952.

[22] J. Hua *et al.*, "Bandwidth-expanded high-linearity Doherty power amplifier with improved AM–AM and AM–PM characteristics," *IEEE Transactions on Microwave Theory and Techniques*, vol. 73, no. 12, pp. 10415–10428, 2025, doi: 10.1109/TMTT.2025.3609778.

[23] R. Liu, H. Jia, L. Qi, and A. Zhu, "A 24-to-30-GHz GaN MMIC Doherty power amplifier using reduced peaking intrinsic output impedance for bandwidth extension," *IEEE Microwave and Wireless Technology Letters*, 2025, doi: 10.1109/LMWT.2025.3528628.

[24] J.-H. Feng, T.-Y. Cheng, H.-T. Dong, L.-S. Wu, and J. Mao, "A 25-to-34-GHz Doherty power amplifier with reconfigurable output network," *IEEE Microwave and Wireless Technology Letters*, vol. 35, no. 9, pp. 1352–1355, 2025, doi: 10.1109/LMWT.2025.3569562.

[25] Y. Yin *et al.*, "A 1.7–2.5-GHz GaAs MMIC Doherty power amplifier with an ultrawideband output network for mobile terminals," *IEEE Microwave and Wireless Technology Letters*, vol. 35, no. 12, pp. 2061–2064, 2025, doi: 10.1109/LMWT.2025.3604457.

[26] J. Chen, J. Pang, R. Gao, S. Liu, G. Zhang, and A. Zhu, "Fully integrated GaN three-stage Doherty power amplifier based on continuous mode for 6G broadband application," *IEEE Transactions on Microwave Theory and Techniques*, vol. 74, no. 7, pp. 6208–6220, 2026, doi: 10.1109/TMTT.2026.3685688.

[27] "Analysis and design of a broadband filtering Doherty power amplifier incorporating harmonic suppression post-matching network," *IEEE Transactions on Microwave Theory and Techniques*, vol. 74, no. 1, pp. 753–767, 2026, doi: 10.1109/TMTT.2025.3619501.

[28] H. Li *et al.*, "Generalized design approach of broadband Doherty power amplifiers with extended back-off range without postmatching network," *IEEE Microwave and Wireless Technology Letters*, vol. 36, no. 4, pp. 589–592, 2026, doi: 10.1109/LMWT.2025.3639227.

[29] O. A. Iupikov, W. Hallberg, R. Maaskant, C. Fager, R. Rehammar, K. Buisman, and M. V. Ivashina, "A dual-fed PIFA antenna element with nonsymmetric impedance matrix for high-efficiency Doherty transmitters: Integrated design and OTA-characterization," *IEEE Transactions on Antennas and Propagation*, vol. 68, no. 1, pp. 21–32, 2020, doi: 10.1109/TAP.2019.2938738.

[30] O. A. Iupikov, J.-R. Perez-Cisneros, P. Meyer, D. Akesson, R. Maaskant, K. Buisman, R. Rehammar, C. Fager, and M. V. Ivashina, "A cavity-backed

patch antenna with distributed multi-port feeding, enabling efficient integration with Doherty power amplifier and band-pass filter," *IEEE Transactions on Antennas and Propagation*, vol. 69, no. 8, pp. 4412–4422, 2021, doi: 10.1109/TAP.2020.3048529.